NanoImpact 6 (2017) 69–80

Contents lists available at ScienceDirect

NanoImpact

journal homepage: www.journals.elsevier.com/nanoimpact

Biokinetics of nanomaterials: The role of biopersistence

Peter Laux [a,*], Christian Riebeling [a], Andy M. Booth [b], Joseph D. Brain [c], Josephine Brunner [a], Cristina Cerrillo [d], Otto Creutzenberg [e], Irina Estrela-Lopis [f], Thomas Gebel [g], Gunnar Johanson [h], Harald Jungnickel [a], Heiko Kock [e], Jutta Tentschert [a], Ahmed Tlili [i], Andreas Schäffer [j], Adriënne J.A.M. Sips [k], Robert A. Yokel [l], Andreas Luch [a]

[a] German Federal Institute for Risk Assessment, Department of Chemical and Product Safety, Max-Dohrn-Strasse 8-10, 10589 Berlin, Germany
[b] SINTEF Materials and Chemistry, Trondheim N-7465, Norway
[c] Harvard T. H. Chan School of Public Health, Boston, MA, USA
[d] IK4-Tekniker, Tribology Unit, Iñaki Goenaga 5, 20600 Eibar, Spain
[e] Fraunhofer Institute for Toxicology and Experimental Medicine (ITEM), Department of Inhalation Toxicology, Nikolai Fuchs Strasse 1, 30625 Hannover, Germany
[f] Institute of Medical Physics & Biophysics, Leipzig University, Härtelstraße 16, 04107 Leipzig, Germany
[g] German Federal Institute for Occupational Safety and Health (BAuA), Friedrich-Henkel-Weg 1-25, 44149 Dortmund, Germany
[h] Institute of Environmental Medicine, Karolinska Institutet, Stockholm, Sweden
[i] Department of Environmental Toxicology, Eawag, Swiss Federal Institute of Aquatic Science and Technology, Dübendorf, Switzerland
[j] Institute for Environmental Research, RWTH Aachen University, Aachen, Germany
[k] National Institute for Public Health & the Environment (RIVM), Bilthoven, The Netherlands
[l] Pharmaceutical Sciences, University of Kentucky, Lexington, KY, USA

ARTICLE INFO

Article history:
Received 30 September 2016
Received in revised form 25 February 2017
Accepted 6 March 2017
Available online 22 March 2017

Keywords:
Biokinetics
Dosimetry
Extrapulmonary organs
Granular biopersistent particle without known significant specific toxicity (GBP)
Inhalation

ABSTRACT

Nanotechnology risk management strategies and environmental regulations continue to rely on hazard and exposure assessment protocols developed for bulk materials, including larger size particles, while commercial application of nanomaterials (NMs) increases. In order to support and corroborate risk assessment of NMs for workers, consumers, and the environment it is crucial to establish the impact of biopersistence of NMs at realistic doses. In the future, such data will allow a more refined categorization of NMs. Despite many experiments on NM characterization and numerous *in vitro* and *in vivo* studies, several questions remain unanswered including the influence of biopersistence on the toxicity of NMs. It is unclear which criteria to apply to characterize a NM as biopersistent. Detection and quantification of NMs, especially determination of their state, *i.e.*, dissolution, aggregation, and agglomeration within biological matrices and other environments are still challenging tasks; moreover mechanisms of nanoparticle (NP) translocation and persistence remain critical gaps. This review summarizes the current understanding of NM biokinetics focusing on determinants of biopersistence. Thorough particle characterization in different exposure scenarios and biological matrices requires use of suitable analytical methods and is a prerequisite to understand biopersistence and for the development of appropriate dosimetry. Analytical tools that potentially can facilitate elucidation of key NM characteristics, such as ion beam microscopy (IBM) and time-of-flight secondary ion mass spectrometry (ToF-SIMS), are discussed in relation to their potential to advance the understanding of biopersistent NM kinetics. We conclude that a major requirement for future nanosafety research is the development and application of analytical tools to characterize NPs in different exposure scenarios and biological matrices.

Contents

Abbreviations: ABB, air-blood barrier; AM, alveolar macrophage; BALF, bronchoalveolar lavage fluid; BBB, blood-brain barrier; CRM, confocal Raman spectroscopy; DEE, diesel engine emissions; DEP, diesel exhaust particles; GBP, granular biopersistent particle without known significant specific toxicity; ICP-MS, inductively coupled plasma mass spectrometry; IBM, ion beam microscopy; LALN, lung associated lymph node; MWCNT, multi-walled carbon nanotube; NM, nanomaterial; NOAEC, no observed adverse effect concentration; NP, nanoparticle; PAA, polyacrylamide; PAH, polyaromatic hydrocarbons; PCLS, precision cut lung slices; PEG, polyethyleneglycol; PIXE, proton-induced X-ray emission; PMN, polymorphonuclear neutrophilic leucocytes; PSP, poorly soluble particle; RBS, Rutherford backscattering spectrometry; RES, reticuloendothelial system; TEM, transmission electron microscopy; TG, technical guideline; ToF-SIMS, time-of-flight secondary ion mass spectrometry.

* Corresponding author.
E-mail address: peter.laux@bfr.bund.de (P. Laux).

http://dx.doi.org/10.1016/j.impact.2017.03.003

1. Introduction

The growing production and use of nanomaterials (NMs) in diverse industrial processes, construction, and medical and consumer products is resulting in increasing exposure of humans and the environment. Humans encounter NMs from many sources and exposure routes, including ingestion of food (Szakal et al., 2014), direct dermal contact through consumer products (Gulson et al., 2015; Vance et al., 2015), and by inhalation of airborne NMs (Donaldson and Seaton, 2012). Environmental exposure on the other hand derives mostly from material aging and waste (Mitrano et al., 2015; Neale et al., 2013). Detecting NMs and understanding their kinetics and transformation are of paramount importance to assess their potential hazards and risks for humans and the environment. With respect to risk assessments, knowledge about the influence of biopersistence on the biokinetics and environmental fate of NMs is required for establishing meaningful categorization approaches.

With regard to human exposure, inhalation is considered the most relevant route for consumers and workers alike. Nano-sized respirable particles will access the alveoli, the location of gas exchange and generally the most vulnerable part of the lungs. A small fraction of NMs may cross biological barriers, such as the air-blood barrier (ABB) of the lung. Translocation of NMs was shown to be dependent on material and aggregate size (Kreyling et al., 2009). This was demonstrated by translocation of NMs to secondary organs such as the liver, heart, spleen, or kidney, subsequent to pulmonary uptake (Choi et al., 2010; Kermanizadeh et al., 2015; Kreyling et al., 2013; Moreno-Horn and Gebel, 2014). Kreyling et al. (2013) concluded that the extent of NM translocation is rather low. For risk assessment, knowledge about exposure including total uptake of NMs and retained multiple organ burdens, as well as tissue localization, and responses is necessary. Basic studies on the biokinetics of polymer nanoparticles (NPs) used in therapeutic applications have revealed size, surface characteristics, and shape as important parameters for their biodistribution *in vivo* (Petros and DeSimone, 2010). While liposomes were found to be rapidly cleared by extravasation or renal clearance if their size ranges between 5 and 10 nm, these mechanisms were not effective at entity sizes above 10 nm (Torchilin, 1998; Vinogradov et al., 2002). Larger entities of ~ 100–200 nm on the other hand, are cleared by the reticuloendothelial system (Petros and DeSimone, 2010). From these findings, a narrow size range of 10–100 nm was concluded to be optimal to achieve enhanced permeability and retention for particulate drug carriers (Petros and DeSimone, 2010). Particle binding and uptake by macrophages is largely influenced by opsonization, the adsorption to the particle surface of protein entities capable of interacting with specific plasma membrane receptors. In addition to opsonization, the interaction between particles and blood protein may lead to further effects such as interference with the blood-clotting cascade, a process that may lead to fibrin formation and anaphylaxis because of complement activation. Prevention of opsonization and complement activation may reduce particulate uptake by macrophages (Moghimi et al., 2001). Neutral vesicles were found to poorly activate the complement system (Chonn et al., 1991; Devine and Bradley, 1998) and to circulate longer in rats when compared to equivalent anionic examples (Senior and Gregoriadis, 1982). The impact of protein binding observed in the case of therapeutically used polymer particles is meanwhile recognized for all materials including NMs for which the term “biomolecular corona” was established, reviewed by Monopoli et al. (2012). Elements of such a corona acquired upon the first contact with the physiological environment might prevail on the particle surface during the onward transport of the material as has been shown for polymeric NPs (Cedervall et al., 2007) and silica (Tenzer et al., 2011). Moreover, the corona might impact a particle's capability to cross biological barriers (Monopoli et al., 2012). Corona formation is influenced by the ratio between surface area and protein concentration (Cedervall et al., 2007; Monopoli et al., 2011). The radius of curvature is considered as another key parameter (Cedervall et al., 2007; Dobrovolskaia et al., 2009; Lundqvist et al., 2008; Tenzer et al., 2011; Zhang et al., 2011). In studies with amorphous silica NPs, particle size impacted the quantity of 37% of all proteins identified, including toxicologically relevant candidates (Tenzer et al., 2011). Inhaled silica NPs acquire a corona during their passage through the respiratory tract lining fluid that is different from the one acquired by the same particles in plasma or whole blood. Investigations of the involved proteins indicate opsonization in preparation of particle phagocytosis and clearance from the lungs (Kumar et al., 2016). Currently most studies on corona formation are carried out with plasma, therefore they are of limited use for inhalation toxicology. In addition, first results indicate that biomolecule absorption from bronchoalveolar lavage fluid (BALF) may equalize particle surface properties (Whitwell et al., 2016).

Under real-life conditions, the majority of airborne NMs appear in agglomerated form. Such agglomerates behave like larger particles with respect to lung deposition, and hence it is crucial to understand where and when (*e.g.* in the product formulation, during aerosolization, or in the lung lining fluid) agglomeration occurs (Aalapati et al., 2014; Konduru et al., 2014; Methner et al., 2010; Morfeld et al., 2012; Pauluhn, 2009b; Seipenbusch et al., 2008; Srinivas et al., 2011). Even agglomerated NMs have almost the same high surface area as primary particles; they induce stronger effects per unit mass than larger microparticles. A contentious issue is the potential deagglomeration of NMs. One side argues that currently there is no evidence and that it is unlikely with respect to the underlying knowledge of physical behavior that NMs deagglomerate in biological milieus (Creutzenberg et al., 2012a; Levy et al., 2012; Preining, 1998). The other side counters that deagglomeration in the lung may occur for some, but not necessarily for all NMs (Mercer et al., 2013; Oberdörster et al., 1992a), keeping in mind the many possible, yet untested, NMs.

In addition to agglomeration, particle dissolution is increasingly recognized as a fundamental parameter influencing inhalation toxicity due to the reduction of particle size and related changes of dissolution kinetics (Pauluhn, 2014a). Since dissolution of metal oxide NMs *in vivo* varies widely, it has to be critically evaluated in each case whether the metal component detected in secondary organs following inhalation arrived there as the original NM or if the original NM dissolved in the lungs or distal to the ABB and then the ions translocated. Recently developed analytical methods allow for a sensitive detection of both particulate and dissolved fractions, which is important but rarely reported.

So far, there has been no valid evidence that NMs show hazards that are different from bulk materials (Donaldson and Poland, 2013; Gebel et

al., 2014). However, the issue remains open since the occupational exposure to materials, summarized as granular biopersistent particles without known significant specific toxicity (GBP) (Roller and Pott, 2006) at concentrations below existing exposure limits correlates with the development of lung diseases (Cherrie et al., 2013; Kuempel et al., 2014). Moreover, epidemiology or studies of chronic effects of engineered NMs are scarce. GBP materials are also referred to as poorly soluble particles (PSPs) (Borm et al., 2015) or poorly soluble low toxicity dusts (Dankovic et al., 2007). In the following, recent studies on NM biokinetics and biopersistence are discussed in relation to potential toxicity. We further present results achieved with new analytical techniques and their potential benefit for the elucidation of *in vivo* biopersistence.

2. The overload concept of particle inhalation and carcinogenicity

Potential carcinogenicity of biopersistent NMs is of concern. The mode of action of GBP materials and the sensitivity of different animal models to lung cancer has been extensively discussed. In the late 1980s, a hypothesis on the mode of action of chronic lung toxicity was developed for dusts, which were called nuisance dusts at that time (Morrow, 1988). Dust over-loading by GBP was defined by Morrow as the failure of alveolar macrophages (AM) to remove dust due to the loss of AM motility. According to Morrow increasing dust loading was associated with a progressive reduction in particle clearance from the deep lung. He postulated that if the particulate volume in an AM exceeded 6% of the AM volume, the overload effect appears to be initiated in the rat. Complete cessation of AM-mediated clearance occurs when the phagocytosed particle volume reaches about 60% of the AM volume, as demonstrated in a subsequent study with 3 and 10 μm polystyrene particles (Oberdörster et al., 1992b).

When testing the applicability of the volumetric overload hypothesis for PSPs, Oberdörster et al. (1994) concluded that the surface area of phagocytized nano- and microparticles correlates better with the diminished particulate matter clearance kinetics than the phagocytized particle volume. Regarding the particle volume, void spaces between the packed particles inside AMs have to be considered, *i.e.*, it is not the material density but the packing density that determines the volume. However, even with a void space correction, Oberdörster et al. (1994) concluded that the phagocytized volume did not show a good correlation with impaired particle clearance. This conclusion was based on an experiment in which rats were exposed by inhalation for twelve weeks to the same high concentration (23 mg/m^3) of either nano- or micro-sized titanium dioxide (TiO_2) or crystalline SiO_2 (quartz) particles (Oberdörster et al., 1994). Inhalation was followed by intratracheal delivery of radioactive tracer particles. However, this conclusion is subject to debate regarding the correction of the biologically relevant void spaces. The agglomerate volume of ultrafine TiO_2 is 1.6 g/cm^3, the material density is 4.3 g/cm^3 (Pauluhn, 2011). The packing density in AMs may be assumed to be even more different due to the fact that in addition void space between agglomerates in AMs also has to be taken into account. During the 180-day post-exposure period in the study of Oberdörster et al. (1994), lung clearance of the nano-TiO_2 was 8-fold slower *versus* only 2-fold slower in micro-TiO_2 exposed rats compared to unexposed controls. Oberdörster et al. (1994) concluded that the diminished clearance correlated with TiO_2 surface areas, confirming the PSP status of both nano- and micro-TiO_2. Quartz, as a PSP of high cytotoxicity, at much lower lung burdens induced an almost 30-fold retardation of test particle clearance (Oberdörster et al., 1997). However, a different opinion is that this result may also be explained by the lower clearance rate for the ultrafine TiO_2 due to a higher total agglomerate volume of the inhaled material. The void space in agglomerates of nano-sized primary particles generally represents a relevant volume portion of the total agglomerate. This leads to a higher volume load in the AMs. It may be estimated that the total volume of nano-TiO_2 was 4-fold that of the micro-TiO_2. This may also explain the slower clearance of nano-TiO_2 compared to the micro-TiO_2 found in Oberdörster et al. (1994).

Recent research suggests that surface area may be the optional dose metric to explain the acute effects of instilled or inhaled particles, but not for repeated dosing leading to inflammation (Pauluhn, 2014b; Schmid and Stoeger, 2016). Some authors have suggested that repeated dosing leading to inflammation may be better explained by particle agglomerate volume (MAK commission, 2014; Pauluhn, 2011). Supporting particle agglomerate volume as relevant dose metric and not surface area, the relative level of polymorphonuclear neutrophilic leucocytes (PMN) in the BALF of rats at 11 months post-exposure was found to be almost five times lower with high surface-area carbon black in comparison to low surface-area carbon black at the identical surface area concentration (dose adjusted accordingly; 7 mg/m^3 high surface-area carbon black *vs.* 50 mg/m^3 low surface-area carbon black) (Elder et al., 2005).

In 2015, a health-based reference inhalation value for workplace exposure to nano-sized GBP was derived based on the avoidance of threshold-dependent sustained inflammatory effects in the lungs (Committee on Hazardous Substances, 2015). For the derivation of the reference value, well performed and reported inhalation studies with TiO_2 (Bermudez et al., 2004; Creutzenberg, 2013), AlOOH (Pauluhn, 2009b) and carbon black Printex® 90 (Elder et al., 2005) were evaluated. Lung inflammation was investigated as the relevant toxicological endpoint and no observed adverse effect concentration (NOAEC) values were determined based on induction of PMNs in the BALF. For the derivation of the reference value, two different approaches were employed. The first approach according to Technical Rule 901 (AGS, 2010) recommends standard factors for time extrapolation, a reduced variability factor of 3 in consideration that rats are rather sensitive to particle-induced lung inflammation, and the increased respiratory volume of a worker. In a second approach, described in detail in Technical Rule 910 (AGS, 2016), particle deposition is modeled using the Multiple-Path Particle Dosimetry model (MPPD version 2.11) and calculation of a human equivalent concentration based on the data from the respective animal experiments. The evaluation came to the conclusion that particle agglomerate volume was the best dose metric explaining the chronic inflammation of nanoscaled GBP/PSP. This was based on comparing either particle agglomerate volume or specific surface area to derive reference values from each of the single inhalation studies included in the evaluation. In case of using particle agglomerate volume as dose metric, the reference values derived from each study generally differed by a factor of 2. In case of using specific surface area as dose metric the derived reference values differed by one order of magnitude. Compared to the occupational exposure limit for microscaled GBP, the inflammatory potency of nano-sized GBP was higher by a factor of 4 when referring to mass concentration. The mode of action was assumed to be identical for nanoscaled and microscaled GBP. The nanoscaled materials exhibit a higher portion of void spaces in their agglomerates and thus possess a higher displacement volume in alveolar macrophages when comparing identical mass concentrations, leading to a higher inflammatory potency.

On the other hand, surface area was considered by others as the most appropriate metrics to estimate the biologically effective dose that causes the toxic effect (Donaldson et al., 2013). From subchronic inhalation testing of TiO_2 and $BaSO_4$ particles in Wistar rats, a threshold of 1 cm^2 particle surface area per cm^2 proximal alveolar region was concluded for the onset of inflammation based on PMN activation in the BALF (Donaldson et al., 2008).

A clear-cut threshold for overload cannot be derived, because particle clearance from the lung decreases in a linear fashion with increasing dust load (Roller, 2003). The consequence of higher dust loading is chronic inflammation mediated by AMs and neutrophils in the deeper airways. Lung carcinogenicity and other lung abnormalities are the consequence of chronic inflammation, which was assumed by some researchers to be species-specific for the rat as hamsters and mice did

not show lung tumors after GBP exposure. Others argued that the latter species may not be adequate indicators for human lung carcinogenicity. For instance, the human carcinogens benzo[*a*]pyrene and vinyl chloride did not show evidence of carcinogenicity after inhalation in hamsters, and mice did not show evidence of carcinogenicity after crystalline silicon dioxide (SiO_2) exposure (Mauderly, 1997). Human epidemiology so far does not indicate a lung carcinogenicity of GBP, *e.g.*, carbon black, TiO_2, or coal dust (IARC, 1997; IARC, 2010). There is wide consensus that diesel engine emissions (DEE) can cause lung cancer in humans (Health Effects Institute, 2015; IARC, 2014). This effect is caused by diesel exhaust particles (DEP) which are nano-sized GBP. It was first assumed that polyaromatic hydrocarbons (PAH) adsorbed to DEP play a relevant role in lung carcinogenicity (Schenker, 1980; U.S. EPA, 2002). However, quantitative evaluations show that the PAH levels adsorbed to DEP are two to three orders of magnitude too low to explain the lung carcinogenicity mediated by DEE (Gebel, unpublished). Thus, lung carcinogenicity in rats and humans is mediated by DEP, *i.e.*, the nano-sized elemental carbon core particle, and not by PAH. As a consequence, it is rather questionable whether lung tumors after chronic inhalation exposure to GBP are specific to the rat only. It remains to be clarified whether the underlying mode of action can be interpreted to be threshold-like and at which definite dose such a threshold may be set.

Based on data from studies in animals and humans, dosimetric risk extrapolation to humans (Oberdörster, 1989) has to consider additional species differences related to the biokinetics of inhaled particulate materials. These include the existence of interstitial lung clearance pathways for both spherical and fibrous particles to the pleural space and subsequent clearance *via* parietal pleura stomata (Donaldson et al., 2010); the finding of lung tumor induction following multi-walled carbon nanotube (MWCNT) inhalation in rats (Kasai et al., 2016; Sargent et al., 2014); and the greater interstitial compartmentalization of retained particles in primates *versus* rodents (Gregoratto et al., 2010; Nikula et al., 1997; Nikula et al., 2001).

In conclusion, AM function to clear retained particles of low biosolubility is a sensitive indicator of adverse effects and applies to both high- and low-toxicity particles. AM volumetric load may be a useful indicator of lung overload for PSP microparticles. Other hypotheses consider the dosimetric particle surface area to be more universally applicable to both nano- and microparticles. However, regardless of what parameter is applied, the determination of pulmonary retention half-times of particles as a key indicator of AM clearance function to characterize overload is essential for confirmation of the overload hypothesis and approval of a threshold-like toxicity. Recent findings on this and further particle distribution are discussed below.

3. Pulmonary retention and biokinetics of nanoparticles following inhalation

In order to test the hypothesis that lung clearance is impaired under overload conditions, a 24-month Combined Chronic Toxicity-Carcinogenicity Study, according to OECD TG 453 (Gebel and Landsiedel, 2013; Ma-Hock et al., 2014; NANoREG, 2015a) in which Wistar rats were exposed to nano-sized CeO_2 over 24 months is currently being performed. The long-term experiment was preceded by a 28-day Subacute Inhalation Toxicity pilot study according to OECD TG 412 (Keller et al., 2014). Here, it was intended to establish appropriate doses, representative for the range of low level environmental and occupational exposure scenarios *via* intermediate particle concentrations, representing a potential threshold above which overload conditions in the lung might exist, to a high exposure concentration for which overload-impaired particle clearance was certainly anticipated. In both inhalation studies, whole body exposure of Wistar rats was performed for 8 h per day and 5 days a week. During the 28-day pilot study, nano-CeO_2 at a low level and expected no observed adverse effect level concentration of 0.5 mg/m^3; a medium level concentration of 5 mg/m^3, and a high level concentration of 25 mg/m^3, which is suspected to cause toxic effects, were applied. Beside the lung burden assessment, an analysis of systemic CeO_2 distribution to other organs, including lung associated lymph nodes (LALN), liver, kidney, blood, spleen, brain, heart, and olfactory bulb was conducted in the frame of the European project NANoREG (2013). The CeO_2 content of organs of the subacute 28-day study was determined on days 28, 30, 36, 62, 92, and 156. CeO_2 organ burdens were calculated from total cerium (Ce) contents [μg/organ] measured by inductively coupled plasma mass spectrometry (ICP-MS) following freeze-drying or plasma-ashing and microwave-assisted wet chemical digestion of the samples. The suitability of the applied method was confirmed by a method equivalence study between BfR and Fraunhofer ITEM (Tentschert and Kock, unpublished) (Fig. 1). Analysis of the lungs from the 28-day pilot study revealed half-times of >80 days for medium (5 mg/m^3) and high (25 mg/m^3) nano-CeO_2 exposure level, and of approximately 69 days for the low level aerosol concentration of 0.5 mg/m^3 (NANoREG, 2015b) (Fig. 2). A typical half-time for pulmonary macrophage-mediated clearance of NMs from the lung of between 50 and 80 days is assumed for GBP particles (Pauluhn, 2011). Half-times above 80 days are an indication of particle overload in the lung or of very insoluble particles. Accordingly, the nano-CeO_2 amounts applied with the medium and high exposure concentrations induced particle overload, as indicated by clearance half-times of >80 days. Based on the lung burden results in the subacute 28-day study, concentrations below 0.5 mg/m^3 were suggested for the application of nano-CeO_2 in the chronic 24-month study in order to prevent particle overload (Keller et al., 2013; NANoREG, 2015a).

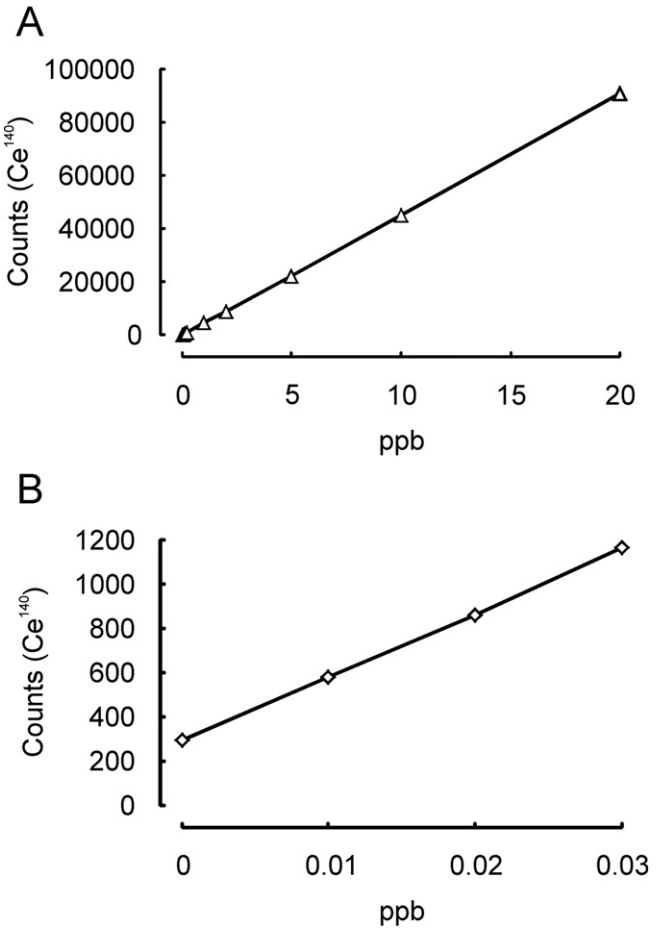

Fig. 1. Method equivalency study for analysis of homogenized liver tissue previously spiked with CeO_2 by inductively coupled plasma mass spectrometry (ICP-MS). (A): linearity at BfR ($R^2 = 0.999977$), (B): linearity at Fraunhofer ITEM ($R^2 = 0.999692$) (Tentschert and Kock, unpublished).

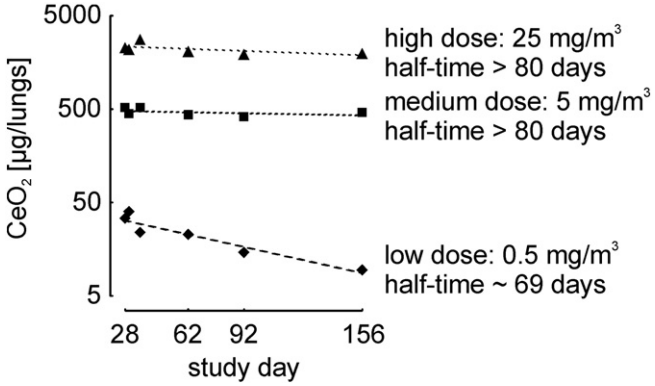

Fig. 2. Post-exposure cerium dioxide (CeO_2) lung burden of rats previously exposed to nano-CeO_2 aerosol for 28 days. Values for low (0.5 mg/m^3), medium (5 mg/m^3) and high (25 mg/m^3) dose group are shown. Each data point represents the mean value of four injections of a single tissue extract (NANoREG, 2015b).

The CeO_2 concentration in the LALNs increased steadily during the post-exposure period of the 28-day pilot study, with the only exception being the low-level exposure group in which the CeO_2 concentration dropped markedly between study day 92 and 156 (Kock, unpublished). This suggests that the lymphatic draining system remained a major mechanism for particle clearance from the lungs and experienced no long-term damage due to nano-CeO_2 exposure at the low exposure concentration (0.5 mg/m^3).

Analysis of further organs from the 28-day pilot study revealed a CeO_2 content in the order: liver > spleen > kidney > blood > heart, brain, olfactory bulb (NANoREG, 2015c). This finding confirms that beyond lung, the liver, spleen, and kidney, in which CeO_2 was recorded in the ppm range, are the main target organs for CeO_2 following inhalation. In contrast, concentrations in blood, heart and brain were in the lower ppb range. The organ burden recorded for lung, liver, spleen, kidney and blood is in accordance with previous results achieved by Geraets et al. (2012), who investigated the systemic distribution of micro- and nanosized CeO_2 in rats following 28-day inhalation: both micro- and nanosized CeO_2 were detected in all investigated extrapulmonary tissues, *i.e.*, liver, spleen, kidney, testis, epididymis, and brain. Like CeO_2, a low systemic distribution was confirmed for three TiO_2 NMs (NM-103, NM-104, NM-105) with different surface characteristics, investigated in a 28-day test. In the study exposure concentrations of 4, 12, and 48 mg/m^3 were applied by a dry powder dispersion technique to rats (Creutzenberg, 2013). AMs were found to be the most prominent compartment of particle detection by transmission electron microscopy (TEM) analysis, while translocation to liver or brain was below the limit of detection. The solubility of the test items was limited to 1–5% by the given conditions of the lung ambience. In inhalation tests with NMs, the agglomeration status varies depending on factors such as the aerosol generation technique, the aerosol concentration, and the dispersion efficiency. These parameters predominantly determine the deposition efficiency and subsequent biokinetic fate. In confirmation of this, no significant differences were recorded regarding the systemic distribution of one micro- and two nanosized CeO_2 materials with primary particle sizes of <5000 nm, 5–10, and 40 nm, occurring with a similar mass median diameter of 1.02, 1.17, and 1.40 µm, respectively, in the test aerosol. NM agglomeration is known to influence the site of NM deposition. Several studies to elucidate the effects of agglomeration and dissolution on translocation to secondary organs are available (Bruinink et al., 2015; Landsiedel et al., 2012). For this reason, a proper design and characterization of the aerosolization is required (Creutzenberg, 2012; Geiser and Kreyling, 2010; Hirsch et al., 2014). The experimental aerodynamic size of a NM can be controlled by selecting various dispersion modes. Beside a pristine dry powder or liquid formulation, a spark generator may be used (Meuller et al., 2012). Individual NPs are not phagocytized highly efficiently by macrophages and may show an enhanced potential for translocation due to their small size (Pauluhn, 2009a). On the contrary, agglomerates consisting of NMs behave aerodynamically in their interaction with macrophages similar to the mechanisms known for fine micro-scaled particles (Braakhuis et al., 2014). In order to investigate if there is deagglomeration *in vivo*, the application of sensitive imaging techniques, allowing for particle detection, is necessary. This would further enable investigation whether different surface characteristics influence particle distribution at the organ and tissue level. Apart from effects of agglomeration, there are several studies that indicate the relevance of biodissolution to NP biokinetics. Two acute inhalation tests, using liquid formulations, focused on this aspect: i.) following deposition of approximately 50 µg Eu_2O_3/rat a very low elemental translocation to remote sites was found with a maximum of 0.9% in liver (Creutzenberg et al., 2016); ii.) at approximately 30 µg of a ^{60}Co-labelled MWCNT/rat the detected elemental translocation was related predominantly to dissolved ^{60}Co with a maximum of 1% in liver (Hackbarth, 2015).

Moreover, in the OECD Testing Programme on Nanomaterials (OECD, 2016), a zinc oxide (ZnO) NM (NM-111) and an amorphous SiO_2 sample (NM-200) were analyzed in 90-day tests for toxic effects and biokinetic behavior using dry powder dispersion (Creutzenberg et al., 2012b). NM-111 showed high solubility and only 2% of the deposited mass was detectable in lungs after the end of the exposure (half-time < 1 week). Other tissue levels were not increased. NM-200 also showed an evident dissolution effect. As a consequence, a total lung clearance half-time of approximately 30 days was calculated, which is well below the established value for particle overload (Pauluhn, 2011). Similar to NM-111, no increase of other tissue levels was observed. In the light of these data it is obvious, that in addition to the well-characterized aerodynamics, the analysis of biopersistence should be an integral part of the test item characterization. Often, a material showing negligible solubility in water exhibits considerable dissolution under physiological conditions. For example, elemental platinum particles (≥4 nm diameter) on Al_2O_3 (≤5 µm diameter) simulating automobile exhaust converters were inhaled by rats in a 90-day study. Up to 30% of the fine dispersed platinum deposited was bioavailable. Using size exclusion chromatography (SEC) in combination with ICP/MS, it was shown that ≥90% of the bioavailable platinum was bound to approx. 80–800 kDa compounds, most likely proteins. In contrast, platinum as a noble metal is 'not soluble' in water (Artelt et al., 1999). Furthermore, Abzhanova et al. (2016) reported high dissolution rates for nickel particles in biological simulants. After 2 h of exposure to artificial saliva or lysosomal liquid, dissolution rates of up to 30 respectively 60% were recorded. Nickel is considered insoluble in water, however its release from metallic jewelry due to dissolution in artificial sweat is well known (Thyssen et al., 2009).

When describing the kinetics of NMs, it is therefore necessary to study the kinetics of particulate and dissolved forms. Beside a diffusion driven translocation, specific transporter proteins were described *e.g.*, for the transport of silver (Bury et al., 1999) and zinc (Kambe et al., 2014) across biological membranes. For Ce, transferrin binding is expected for the trivalent form (Zende-Del et al., 2013) and confirmed for the tetravalent form (Baker et al., 2000; Subramanian and Oomen, 1981). Whereas the kinetics of the particulate form is merely driven by uptake and dissolution in the reticuloendothelial system (RES), the kinetics of molecular compounds and ions is based on diffusion, carrier mediated uptake, and on metabolic transformation. Information on particle dissolution rate in various environments in the body seems to be key to a better understanding of NM kinetics. This also implies that plasma kinetics do not give a proper reflection of tissue kinetics and body burden. Hence, it can be concluded that study designs for molecular compounds, based on plasma kinetics, insufficiently support insight into NM kinetics (Hagens et al., 2007; Riviere, 2009). Chemical analysis together with imaging techniques should be used to clarify whether ionic or particulate species translocate from lungs following inhalation. This integrative analysis is important to allow a conclusive

interpretation of NM biokinetic data in order to estimate whether there is an increased barrier penetration and organ-specific accumulation outside of the lungs in comparison to their respective bulk materials (Kreyling et al., 2009).

4. A comparison between CeO_2 and $BaSO_4$ biokinetics following instillation

By working with radioactively labelled NMs, a complete recovery and exact localization of the applied dose is realized, *albeit* limited to the labelled element (Molina et al., 2014). This has the potential to better predict NM biokinetics compared to common techniques of elemental analysis, such as ICP-MS, which requires sample digestion. Even though CeO_2 and barium sulfate ($BaSO_4$) were both considered GBP, $BaSO_4$ NM had a much shorter half-time following instillation. Experiments were performed with nano-$BaSO_4$, as well as nano-CeO_2 and ionic Ce, all of which were subjected to neutron activation resulting in Ba and Ce becoming the gamma emitters ^{131}Ba and ^{141}Ce, respectively. A limitation of these isotopes for long term studies is their decay half-life, ~12 and 32.5 days, respectively.

Fig. 3A shows the pulmonary clearance of ^{141}Ce for four weeks after intratracheal instillation into rats (Molina et al., 2014). Nano-CeO_2 is slowly cleared from the lungs. Ionic Ce also had a slow clearance from the lungs, consistent with its low elimination in urine and feces and organ retention after systemic injection (Molina et al., 2014; Yokel et al., 2014a). Ce retention following ionic Ce instillation may be attributed to the formation of persistent insoluble cerium phosphates that are then cleared slowly (Berry et al., 1989; Berry et al., 1997). A contributor to the slow clearance of nano-CeO_2 might be dissolution of particles followed by subsequent particle formation.

Nano-$BaSO_4$ had a much shorter half-time (Konduru et al., 2014). Fig. 3B describes translocation of radioactive ^{131}Ba from the lungs to extrapulmonary organs. It compares nano-$BaSO_4$ with nano-CeO_2. The differences are dramatic. Surprisingly, one-third of the instilled dose of Ba appears in other organs, especially bone marrow (Konduru et al., 2014). While it is possible that this represents intact NM translocation across the ABB, particle dissolution and ion transport into the blood and then the bone marrow is a far more likely mechanism.

Overall, ^{141}Ce in nano-CeO_2 or $CeCl_3$ is cleared slowly from the lungs. Ionic Ce is cleared somewhat faster than particles. There is also greater translocation of ^{141}Ce following intratracheal instillation *versus* after gavage (Molina et al., 2014). $^{131}BaSO_4$ has greater bioavailability and is cleared much faster from the lungs than CeO_2. Moreover, extrapulmonary retention of Ba is much higher than of Ce post-instillation (Fig. 3B). CeO_2 and $BaSO_4$ were also found to exhibit very low bioavailability following gavage. Therefore, fur deposition and subsequent grooming during aerosol exposure to nano-CeO_2 or nano-$BaSO_4$ are unlikely to result in retention in other organs.

5. Biokinetics of CeO_2 nanoparticles after infusion: the influence of size and solubility

Since NM toxicity is potentially influenced by their specific biokinetics (Oberdörster et al., 2005; Semmler et al., 2004), there is a need to elucidate the impact of physico-chemical properties on NM distribution *in vivo*. In consideration of recent results on tissue distribution of micro- and nano-sized CeO_2 particles in rats (Geraets et al., 2012), this demand may be considered relevant for microscaled particles alike. The human body is prepared to deal with particles in blood by means of the RES (Arvizo et al., 2010; Card et al., 2008; Kettiger et al., 2013; Sa et al., 2012) and biodegradation in the phagolysosomes (Ernsting et al., 2013; Yu and Zheng, 2015). However, there is insufficient knowledge on how physico-chemical properties of particles, such as size, solubility, and shape affect their kinetics.

A systematic comparison of a commercial 30 nm platelet, and in-house synthesized/extensively characterized citrate-coated ~5, 15, 30,

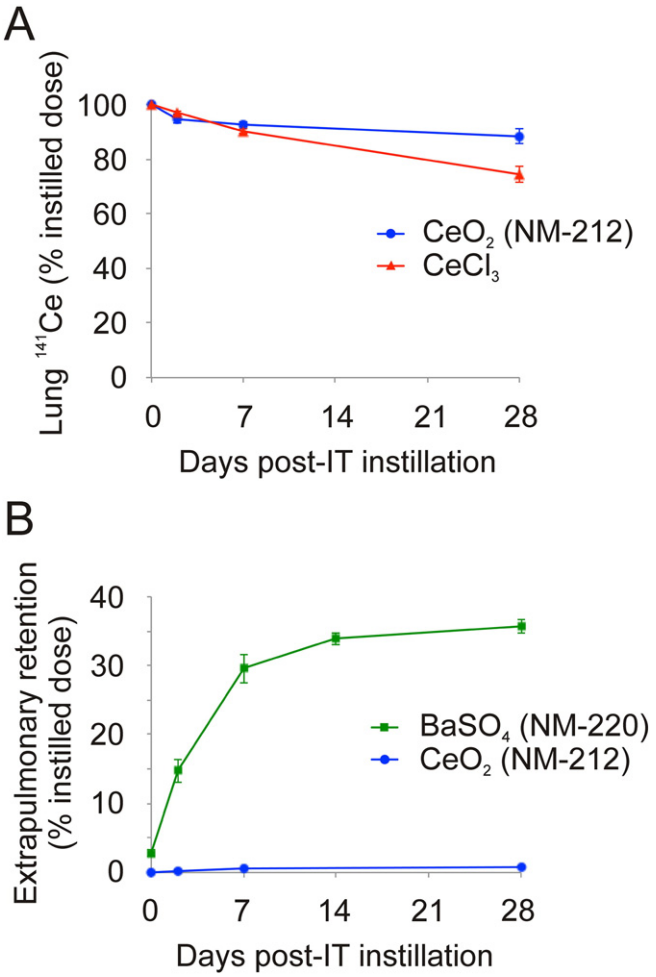

Fig. 3. Biokinetics of neutron activated nanoparticles. (A) Lung clearance of cerium-141 (^{141}Ce) after instillation of cerium-141 dioxide ($^{141}CeO_2$) nanoparticles and cerium-141 chloride ($^{141}CeCl$). Reprinted from Environmental Science: Nano 1, Molina RM, Konduru NV, Jimenez RJ, Pyrgiotakis G, Demokritou P, Wohlleben W, Brain, JD, Bioavailability, distribution and clearance of tracheally instilled, gavaged or injected cerium dioxide nanoparticles and ionic cerium, 561–573, Copyright 2014, with permission from the Royal Society for Chemistry. (B) Extrapulmonary retention of ^{141}Ce and barium-131 (^{131}Ba) after intratracheal instillation of $^{141}CeO_2$ and barium-131 sulfate ($^{131}BaSO_4$) nanoparticles (Konduru et al., 2014; Molina et al., 2014).

and 55 nm polyhedral/cubic CeO_2, and CeO_2 nanorods (10 to 15 × 50 to 460 nm) was performed utilizing intravenous infusion of rats. Up to 750 mg/kg commercial nano-sized CeO_2 was tolerated (Yokel et al., 2009). The initial clearance half-time of Ce from the blood after intravenous infusion of 15, 30, and 55 nm CeO_2 was <10 min (Dan et al., 2012b). Nano-CeO_2 of 5 nm circulated much longer (Dan et al., 2012b). Ce blood concentration increased a few hours after intravenous infusion of the 15 and 30 nm CeO_2, a behavior not seen with the 5 or 55 nm CeO_2 (Dan et al., 2012b). In the first 2 weeks after 30 nm CeO_2 infusion 0.01% was excreted in urine and 0.5% in feces (Yokel et al., 2012). Similarly, urinary Ce was not detected after oral, intraperitoneal, or intravenous administration of 3 to 5 nm CeO_2 to mice (Hirst et al., 2013). Clearance of nano-CeO_2 was primarily into the liver (which contained the greatest percentage of the dose), spleen, and bone marrow (Yokel et al., 2012; Yokel et al., 2013). Lower Ce levels were detected in 13 other organs. This biodistribution pattern is similar to that seen after intravenous administration of 5.6 nm 3-aminopropylsilyl-anchored *N*-succinimidyl 4-[^{18}F]fluorobenzoate coated nano-CeO_2 to rats (Rojas et al., 2012), and 2.9 nm citrate-EDTA coated nano-CeO_2 to mice (Heckman et al., 2013). There was little Ce decrease over 90 days other than some from the liver (Yokel et al., 2012), whereas Ce levels in the liver, spleen, brain, and kidney of mice decreased over 5 months

after intravenous administration of 2.9 nm citrate-EDTA coated nano-CeO_2 (Heckman et al., 2013). Distribution and persistence were similar after 11 *versus* 85 mg/kg 5 nm CeO_2 and 6 *versus* 85 mg/kg 30 nm CeO_2, suggesting lack of clearance mechanism overload (Yokel et al., 2014b). Distribution and persistence after 1 *versus* 5 daily 11 mg/kg 5 nm CeO_2 intravenous infusions were similar, indicating no compensatory mechanisms (Yokel et al., 2014b). CeO_2 nanorod organ distribution and retention were similar to polyhedral/cubic CeO_2, suggesting no appreciable shape effect (Yokel et al., 2014b). Brain CeO_2 association was not concentration- or infusion-duration-dependent following carotid artery 5 nm CeO_2 infusions, pointing to a saturated mechanism of brain uptake (Dan et al., 2012a). When separated from brain parenchyma, blood-brain barrier (BBB) cells contained >99% of the nano-CeO_2, consistent with TEM observations of little to no nano-CeO_2 distribution into brain parenchyma (Hardas et al., 2010; Yokel et al., 2009; Yokel et al., 2013). Following their intravenous and intracarotid administration, 5 nm CeO_2 were associated with the BBB luminal surface (Dan et al., 2012a; Hardas et al., 2010). Release from the vascular luminal surface, perhaps due to protein coating, may result in its re-circulation in blood, perhaps explaining the Ce increase after intravenous infusion of the 15 and 30 nm CeO_2 (Dan et al., 2012b). Nano-CeO_2 accumulated as micron-sized intracellular agglomerates in Kupffer cells, hepatocytes, hepatic stellate cells, and spleen red pulp (Tseng et al., 2012; Yokel et al., 2013). Ninety days after 30 nm cubic CeO_2 intravenous infusion, clouds of 1 to 3 nm CeO_2 were seen in the liver near the accumulated CeO_2 particles that now had rounded corners and edges (Graham et al., 2014). The 1 to 3 nm CeO_2 exhibited enhanced Ce^{3+} and phosphorus suggesting partial dissolution of nano-sized CeO_2 particles followed by cerium phosphate precipitation. Hence, bioprocessing produced a more stable, anti-oxidant form of nano-CeO_2. Intravenous nano-CeO_2 is acutely quite non-toxic, but persists and is bioprocessed by unknown mechanisms to Ce-containing products that may have different biological effects. Identification of the relevant Ce speciation occurring *in vivo* might lead to the elucidation of potential biological effects.

6. New imaging techniques for nanomaterial characterization *in vitro* and *ex vivo*

Analytical quantification of NMs in digested tissue or in *in vitro* cultures by methods such as ICP-MS can only provide limited information on size, shape, and speciation of particles and especially no quantification of the effective dose at the cellular level. At the same time, information on deagglomeration and biopersistence is urgently required for the establishment of NM biokinetics.

As described previously, high-resolution TEM was successfully applied for imaging of nano-CeO_2 alteration *in vivo* (Graham et al., 2014). A variety of further imaging techniques were recently adapted to visualize NPs and NP aggregates in biological matrices such as time-of-flight secondary ion mass spectrometry (ToF-SIMS) (Haase et al., 2011), ion beam microscopy (IBM) (Zhou et al., 2014), and confocal Raman microscopy (CRM) (Romero et al., 2011b). ToF-SIMS, a method originally developed in material science (Fletcher et al., 2011), enables the chemical identification of CeO_2 particles in tissues based on the detection of the CeO^+ ion; it provides a size estimation with a spatial resolution down to 60 nm on nanoscale depth (Holzweber et al., 2014) and a distribution of NMs in the z-direction with an accuracy of about 9 nm. ToF-SIMS was applied to analyze cells of the micro algae *Pseudokirchneriella subcapitata* following a 72 h exposure to poly-acrylic acid stabilized nano-CeO_2. The results showed that 38% of the total Ce directly associated with the algal cells. Moreover, a significant change in the chemical composition of the cell wall was observed, indicating a significant oxidative stress response within NP exposed cells (Booth et al., 2015). IBM techniques, such as proton-induced X-ray emission (PIXE) and Rutherford backscattering spectrometry (RBS), on the other hand, allow for spatially resolved elemental imaging and quantitative analysis at the single cell level with lateral resolution of about 1 μm. By the combination of PIXE and RBS, quantification of the genuine concentration of NMs in single cells and of metabolically relevant cellular elements such as phosphorus, sulfur, calcium, potassium, zinc, and iron with a sensitivity at the ppm range becomes possible (Llop et al., 2014; Reinert et al., 2011; Zhou et al., 2014). Moreover, RBS can reveal the distribution of NMs in the z-direction with an accuracy of about 50 nm (Lopis, unpublished). The method allows thus to distinguish between NMs which are internalized or only attached to the plasma membrane from the outside. Additionally, the molecule-based imaging technique CRM provides 3D chemical composition images with a lateral resolution of about 260 nm. CRM reveals not only the 3D NM distribution but also their 3D co-localization with cell compartments and biomolecules (Chernenko et al., 2009; Estrela-Lopis et al., 2011; Haase et al., 2011; Matthaus et al., 2008; Romero et al., 2011a; Romero et al., 2010; Romero et al., 2013; Silge et al., 2015).

The feasibility to locate and characterize CeO_2 particles in lung tissue sections by ToF-SIMS and PIXE was investigated using samples of the 28-day pilot study mentioned above (Gebel and Landsiedel, 2013; Ma-Hock et al., 2014). ToF-SIMS analysis of deparaffinized tissue sections showed the occurrence of nano-CeO_2 agglomerates in lung (Fig. 4) and liver (Jungnickel, unpublished) of animals of the highest dose group (Gebel and Landsiedel, 2013; Ma-Hock et al., 2014). The detected clusters were not equally distributed; a higher density of particles was found in lung compared to liver. The application of PIXE on lung tissue slices of animals of the highest dose group revealed a predominant occurrence of CeO_2 particles in AMs located in the lumen of the alveoli with a mean concentration of about 30,000 ppm (Merker and Lopis, unpublished) (Fig. 5). Furthermore, the images revealed a rather inhomogeneous CeO_2 distribution in the alveolar septum. The analysis of 30 alveoli revealed a mean CeO_2 concentration of about 1700 ppm and "hot spots" containing >5000 ppm. The mean Ce concentration in the alveolar septum was comparable in magnitude with that of phosphorus and sulfur (Merker and Lopis, unpublished).

Nano-CeO_2 was also detected in close vicinity to erythrocytes in blood vessels in the lung after 28 days of nano-CeO_2 inhalation (Fig. 4), consistent with nano-CeO_2 on the surface of erythrocytes after 1 h incubation (Hardas et al., 2010) and an increase of the fraction of 15 and 30 nm CeO_2 associated with erythrocytes, white blood cells and platelets over 4 h after their intravenous infusion (Dan et al., 2012b). This might contribute to systemic redistribution of NMs through blood circulation to other organs.

IBM and CRM techniques were further evaluated for their ability to detect the intracellular concentration of elements *in vitro*. In A549 cells, a human alveolar adenocarcinoma epithelial cell line (Giard et al., 1973), the concentration of Ce following application of CeO_2 in a concentration of 10 μg/ml was found to be one order of magnitude higher compared to the alveolar septum (Lopis, unpublished). Comparison of the intracellular effective dose in cultured cells and tissues could help address the *in vitro*/*in vivo* correlation on a quantitative basis (Cohen et al., 2015).

Based on the described findings, ToF-SIMS, IBM and CRM techniques are currently applied to study particle uptake and fate in organ tissues obtained from a combined chronic toxicity/carcinogenicity study (Gebel and Landsiedel, 2013; Ma-Hock et al., 2014; NANoREG, 2015a). While ToF-SIMS investigations are targeting particle identification and accumulation in specific organs, IBM and PIXE studies are capable of providing qualitative and quantitative information on local Ce concentrations in tissues and cells. This approach may reveal whether nano-GBPs accumulate either as distinct particles, aggregates or agglomerates within the tissue, and whether they translocate to the lymphatic system or the bloodstream with subsequent distribution to secondary organs (Kato et al., 2003; Nemmar et al., 2004).

A combined application of such imaging techniques could help introduce the methodology of morphometry (Weibel, 1979) to NP toxicology. The degree and mechanism of uptake, localization, and distribution of NMs in cells and organs are major issues in respect to

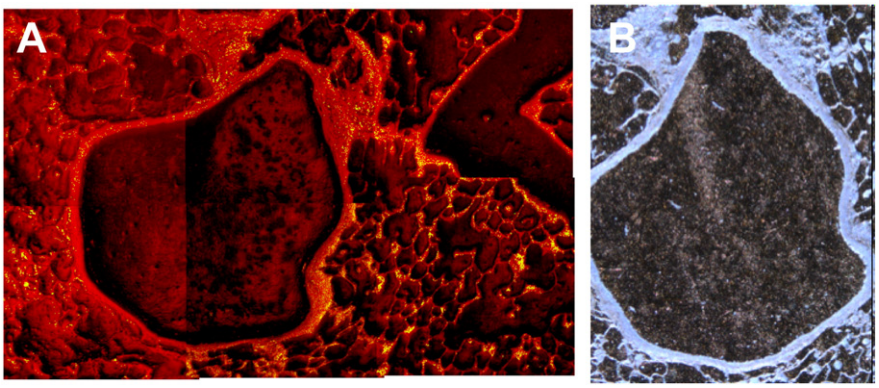

Fig. 4. Detection of cerium dioxide (CeO_2) particle clusters in lung tissue. (A): Time-of-flight secondary ion mass spectrometry image (1.5 mm × 1 mm) of a deparaffinated lung tissue slice from rats previously exposed to CeO_2 aerosol (25 mg/m^3) for 28 days. The total ion spectrum is displayed; yellow dots, signals of the CeO^+ ion are representing CeO_2 particles. (B) Corresponding light microscopy image of A (0.75 mm × 1 mm) (Jungnickel, unpublished).

toxicity and risk assessment of such materials. Addressing these issues requires establishing innovative high-resolution dosimetry and imaging methods, which are especially suitable for study of NMs within their biological environment *in vitro* and *in vivo*.

Application of techniques such as ToF-SIMS, CRM, and IBM to organs from animal experiments is currently limited, as most of the tissue samples are required for histopathology and quantitative element analysis in previously digested samples. In order to analyze the native status of NM distribution, a conservation of the living cell status is necessary, which can be achieved by techniques such as plunge freezing (Comolli et al., 2012).

However, despite the limited availability of tissue material, fast freezing techniques are not established on a broad basis yet. On the other hand, these techniques are common for alternative test systems such as precision cut lung slices (PCLS) that can be used as a toxicity screening method for chemicals and particles (Watson et al., 2016). The advantages of using living lung slices include preservation of organ structure, lower cost, fewer animals, and especially assays with high throughput and high content. Cryopreservation helps to preserve viability, metabolism, structure, and airway function. Results achieved with PCLS are consistent with *in vitro* assays and *in vivo* animal models. Thus, PCLS might be used as a suitable model for the investigation of particle biokinetics in combination with imaging techniques.

7. Elucidation of nanomaterial biokinetics by physiologically-based modeling

The potential of *in silico* tools in biokinetics has received increasing attention. As an ultimate goal, a generic, physiologically-based pharmacokinetic (PBPK) model is envisaged, that is able to describe the biodistribution of any NM for any exposure route. Such a model would offer the opportunity for a comparative internal dosimetry, helping to understand effects observed in rodents and their potential relevance to humans (Sweeney et al., 2015).

A three-compartment model including alveolar, interstitial, and hilar lymph node compartments was developed in order to predict the long-term retention of particles in the lungs of coal miners (Kuempel et al., 2001a; Kuempel et al., 2001b). Particle sequestration, excluding a portion that is translocated to lung interstitium and LALN from macrophage mediated clearance was found essential for describing the disposition of GBP in lungs of humans with chronic occupational exposure. Adjustment for these differences in particle kinetics becomes necessary when using rodent data for prediction of human lung diseases. In an approach to describe retention and clearance of respirable crystalline silica, Tran et al. (2002) have extended the human model structure established by Kuempel and coworkers. Since reduction of particle clearance in the underlying inhalation studies was attributed to AMs, these are considered as a further compartment in their approach. Based on this refined model, threshold doses of crystalline silica that initiate inflammation and fibrosis were set at 0.20 ± 0.19 and 1.96 ± 0.12 mg, respectively. Moreover, an extended number of compartments representing particle mass on the alveolar surface, inside macrophages, interstitial space, in the lymph nodes, in the olfactory and in the upper airways region was developed (MacCalman and Tran, 2009; MacCalman et al., 2009). Data were acquired from *in vivo* studies in rats with iridium and silver NPs (Fabian et al., 2008; Semmler et al., 2004; Takenaka et al., 2001). Endotracheal instillation and inhalation,

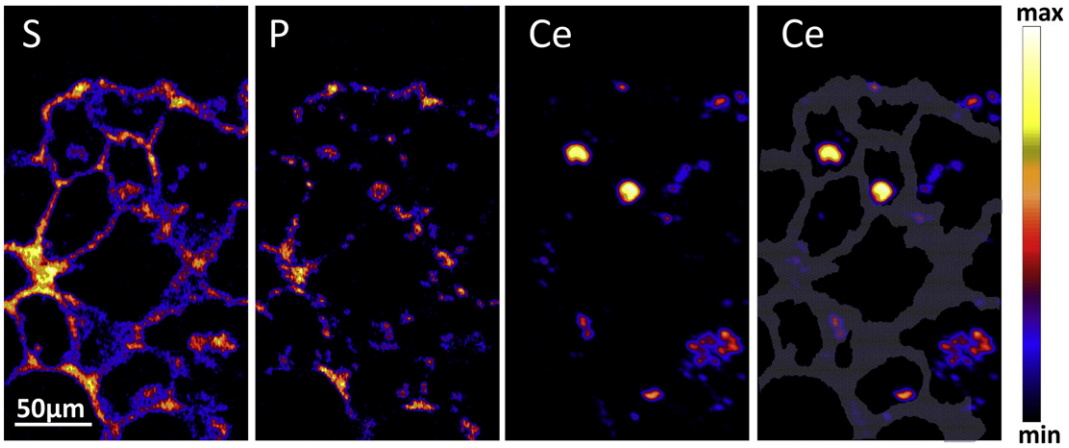

Fig. 5. Proton-induced X-ray emission (PIXE) images of sulfur (S), phosphorus (P), and cerium (Ce) distribution in alveoli of lung tissue from rats, which had been exposed to cerium dioxide (CeO_2) aerosol (25 mg/m^3) for 28 days. The grey area outlines the alveolar septum. (Merker and Lopis, unpublished).

the different exposure methods applied respectively in these studies, showed an influence on optimal parameter estimates and were mentioned as one difficulty for a validation (MacCalman et al., 2009). A recalibration of this model by a Bayesian population analysis for improving assessment of parameter variability and uncertainty was conducted by Sweeney et al. (2015). By this approach it became feasible to calibrate the model for different data sets, in addition to the studies used by MacCalman et al. (2009) and MacCalman and Tran (2009) additional studies with iridium, carbon, and silver NPs were identified as useful (Kreyling et al., 2009; Kreyling et al., 2002; Lankveld et al., 2010). A predominant influence of the exposure route on biokinetics was also confirmed in preliminary modeling efforts using nano-CeO_2 (Carlander, unpublished). To avoid the complexities of the oral and pulmonary routes, several recent approaches have investigated the biodistribution of intravenously administered NMs. The PBPK model developed by Li et al. (2014) consists of ten compartments interconnected *via* the blood circulation: arterial blood, venous blood, lungs, spleen, liver, kidneys, heart, brain, bone marrow, and rest of body. Each compartment has three sub-compartments corresponding to capillary blood, tissue, and phagocytizing cells. The exchange of NPs between blood and organs is described as flow- and diffusion-limited processes. The permeability coefficient of the brain compartment is set to zero assuming an efficient BBB. The NM mass transfer in each compartment is expressed as a first-order differential equation and the overall biodistribution profile is obtained by simultaneous solution of all ten differential equations over time. The model was optimized by best fit to intravenous rat experimental data obtained with polyethylene glycolylated polyacrylamide (PAA-PEG) NMs (Li et al., 2014). Carlander et al. (2016) have slightly modified this model for simultaneous predictions of the following NMs: PAA-PEG, uncoated PAA, gold and TiO_2 NMs. These NMs were selected since sufficient experimental biokinetic data for optimization are available. Essentially the same model and physiological parameters as above were applied, whereas NM-specific parameters were re-optimized by best fit. All four types of NMs were adequately described in their biokinetic behavior by the model, despite extensive differences in physico-chemical properties and biokinetic profiles. Furthermore, the simulations demonstrated that the dose exerts a profound impact on the biokinetics, since saturation of the phagocytic cells at higher doses becomes a major limiting step. The fitted model parameters that were most dependent on NM-type included blood:tissue partition coefficients and the rate constant for phagocytic uptake (Carlander et al., 2016). Since only four types of NMs with several differences in characteristics were used, the relationship between these characteristics and the NM-dependent model parameters could not be elucidated and more experimental data are required. Intravenous biodistribution studies with associated PBPK analyses would provide the most insight (Kreyling et al., 2009; Kreyling et al., 2002; Semmler-Behnke et al., 2007; Semmler et al., 2004; Sweeney et al., 2015). Biopersistence and solubility have been identified as important parameters of biokinetic modeling (Bachler et al., 2013; Lankveld et al., 2010; Sweeney et al., 2015) but need to be aligned with other aspects such as agglomeration, corona formation and phagocytosis. Further use of experimental data in PBPK modeling can help to understand the interaction between these different mechanisms and their influence on the biokinetics of NMs.

8. Conclusions

Detection and quantification of NMs and their transformation presents a challenge for human toxicology. The strong influence of physico-chemical properties, in particular *in situ* solubility, on the biokinetics of NMs following their inhalation requires a focus on pulmonary nanotoxicology (Donaldson and Poland, 2013). Properties of particles, aggregates, and agglomerates, such as size and aerodynamic and thermodynamic diameter, drive kinetic processes like pulmonary deposition and dissolution. The relevance of lung overload for lung tumor formation remains a difficult but important issue for risk assessment of biopersistent particles, even those without known specific toxicity. Correspondingly, the need to characterize the particle fate under physiological conditions by qualitative and quantitative analysis remains a significant need. As shown for the example of rat lung slices of animals previously exposed to a nano-CeO_2 aerosol, imaging techniques such as ToF-SIMS – recently adapted to biological matrices – can provide a distinct identification and morphological characterization of particles *in vivo*. Tools such as PIXE and neutron activation on the other hand enable precise substance quantification in different organs and even within cells. A targeted combination of such methods may allow for further progress of categorization approaches and refinement of PBPK modeling and thus reduce animal testing. In the case of nano-CeO_2, some biotransformation to cerium phosphate NPs during the retention, primarily in reticuloendothelial system organs, is indicated by results obtained with intratracheal and intravenous administration.

Acknowledgments

The authors acknowledge support from the EU FP7 project 'NANoREG' (Grant Agreement number 310584). The authors wish to thank this project for financial support of their research and for periodic teleconferences and meetings. The authors further wish to thank G. Oberdörster for the scientific discussions.

JD Brain: Participants in this research included Ramon Molina, Tom Donaghey, Nagarjun Konduru Venkata, Christa Watson (Harvard); Wendel Wohlleben, Robert Landsiedel (BASF); Rama Krishnan, Sumati Ram-Mohan (BIDMC, Boston): Supported by NIH Grant ES-OOOOO2 and by BASF.

RA Yokel: Participants in this research included Eric A. Grulke, D. Allan Butterfield, Jason Unrine, and Uschi Graham (University of Kentucky) and Michael T. Tseng (University of Louisville). Supported by US-EPA STAR Grant RD-833772.

I. Estrela-Lopis: Participants in this research included Carolin Merker.

G Johanson: Ulrika Carlander participated in this project, supported by the Swedish Research Council for Health, Working Life and Welfare (FORTE) Grant 2010-0702.

A.M. Booth: Supported by Polish-Norwegian Research Programme (Project Contract No. Pol-Nor/237761/98/2014) and the Research Council of Norway project (Contract No. 239199/O70).

References

Aalapati, S., Ganapathy, S., Manapuram, S., Anumolu, G., Prakya, B.M., 2014. Toxicity and bio-accumulation of inhaled cerium oxide nanoparticles in CD1 mice. Nanotoxicology 8 (7), 786–798.

Abzhanova, D., Godymchuk, A., Gusev, A., Kuznetsov, D., 2016. Exposure of nano- and ultrafine Ni particles to synthetic biological solutions: predicting fate-related dissolution and accumulation. Eur J Nanomed 8 (4), 203–212.

AGS, German Committee on Hazardous Substances, 2010. Begründungen und Erläuterungen zu Grenzwerten in der Luft am Arbeitsplatz, Technical Rule for Hazardous Substances TRGS 901. http://www.baua.de/de/Themen-von-A-Z/Gefahrstoffe/TRGS/Bekanntmachung-901.html (Accessed 24.02.2017).

AGS, German Committee on Hazardous Substances, 2016. Risk-Related Concept of Measures for Activities Involving Carcinogenic Hazardous Substances, Technical Rule for Hazardous Substances TRGS 910. http://www.baua.de/en/Topics-from-A-to-Z/Hazardous-Substances/TRGS/TRGS-910.html (Accessed 24.02.2017).

Artelt, S., Creutzenberg, O., Kock, H., et al., 1999. Bioavailability of fine dispersed platinum as emitted from automotive catalytic converters: a model study. Sci. Total Environ. 228 (2–3), 219–242.

Arvizo, R., Bhattacharya, R., Mukherjee, P., 2010. Gold nanoparticles: opportunities and challenges in nanomedicine. Expert Opin. Drug Deliv. 7 (6), 753–763.

Bachler, G., von Goetz, N., Hungerbuhler, K., 2013. A physiologically based pharmacokinetic model for ionic silver and silver nanoparticles. Int. J. Nanomedicine 8, 3365–3382.

Baker, H.M., Baker, C.J., Smith, C.A., Clyde, A., Baker, E.N., 2000. Metal substitution in transferrins: specific binding of cerium(IV) revealed by the crystal structure of cerium-substituted human lactoferrin. J. Biol. Inorg. Chem. 5 (6), 692–698.

Bermudez, E., Mangum, J.B., Wong, B.A., et al., 2004. Pulmonary responses of mice, rats, and hamsters to subchronic inhalation of ultrafine titanium dioxide particles. Toxicol. Sci. 77 (2), 347–357.

Berry, J.P., Masse, R., Escaig, F., Galle, P., 1989. Intracellular localization of cerium. A micro-analytical study using an electron microprobe and ionic microanalysis. Hum. Toxicol. 8 (6), 511–520.

Berry, J.P., Zhang, L., Galle, P., Ansoborlo, E., Henge-Napoli, M.H., Donnadieu-Claraz, M., 1997. Role of alveolar macrophage lysosomes in metal detoxification. Microsc. Res. Tech. 36 (4), 313–323.

Booth, A., Storseth, T., Altin, D., et al., 2015. Freshwater dispersion stability of PAA-stabilised-cerium-oxide nanoparticles and toxicity towards *Pseudokirchneriella subcapitata*. Sci. Total Environ. 505, 596–605.

Borm, P., Cassee, F.R., Oberdörster, G., 2015. Lung particle overload: old school - new insights? Part Fibre Toxicol 12, 10.

Braakhuis, H.M., Park, M.V., Gosens, I., De Jong, W.H., Cassee, F.R., 2014. Physicochemical characteristics of nanomaterials that affect pulmonary inflammation. Part Fibre Toxicol 11, 18.

Bruininik, A., Wang, J., Wick, P., 2015. Effect of particle agglomeration in nanotoxicology. Arch. Toxicol. 89 (5), 659–675.

Bury, N.R., Grosell, M., Grover, A.K., Wood, C.M., 1999. ATP-dependent silver transport across the basolateral membrane of rainbow trout gills. Toxicol. Appl. Pharmacol. 159 (1), 1–8.

Card, J.W., Zeldin, D.C., Bonner, J.C., Nestmann, E.R., 2008. Pulmonary applications and toxicity of engineered nanoparticles. Am J Physiol-Lung C 295 (3), L400–L411.

Carlander, U., Li, D., Jolliet, O., Emond, C., Johanson, G., 2016. Toward a general physiologically-based pharmacokinetic model for intravenously injected nanoparticles. Int. J. Nanomedicine 11, 625–640.

Cedervall, T., Lynch, I., Lindman, S., et al., 2007. Understanding the nanoparticle-protein corona using methods to quantify exchange rates and affinities of proteins for nanoparticles. Proc. Natl. Acad. Sci. U. S. A. 104 (7), 2050–2055.

Chernenko, T., Matthaus, C., Milane, L., Quintero, L., Amiji, M., Diem, M., 2009. Label-free Raman spectral imaging of intracellular delivery and degradation of polymeric nanoparticle systems. ACS Nano 3 (11), 3552–3559.

Cherrie, J.W., Brosseau, L.M., Hay, A., Donaldson, K., 2013. Low-toxicity dusts: current exposure guidelines are not sufficiently protective. Ann. Occup. Hyg. 57 (6), 685–691.

Choi, H.S., Ashitate, Y., Lee, J.H., et al., 2010. Rapid translocation of nanoparticles from the lung airspaces to the body. Nat. Biotechnol. 28 (12), 1300–1303.

Chonn, A., Cullis, P.R., Devine, D.V., 1991. The role of surface-charge in the activation of the classical and alternative pathways of complement by liposomes. J. Immunol. 146 (12), 4234–4241.

Cohen, J.M., DeLoid, G.M., Demokritou, P., 2015. A critical review of in vitro dosimetry for engineered nanomaterials. Nanomedicine 10 (19), 3015–3032.

Committee on Hazardous Substances, BAuA, 2015. Assessment Criterion (Reference Value) for Granular Biopersistent Particles Without Known Significant Specific Toxicity (Nanoscaled GBP) (Respirable Dust) Generated From Manufactured Ultrafine Particles. http://www.baua.de/en/Topics-from-A-to-Z/Hazardous-Substances/TRGS/pdf/910/nanoscaled-GBP.pdf.

Comolli, L.R., Duarte, R., Baum, D., et al., 2012. A portable cryo-plunger for on-site intact cryogenic microscopy sample preparation in natural environments. Microsc. Res. Tech. 75 (6), 829–836.

Creutzenberg, O., 2012. Biological interactions and toxicity of nanomaterials in the respiratory tract and various approaches of aerosol generation for toxicity testing. Arch. Toxicol. 86 (7), 1117–1122.

Creutzenberg, O., 2013. Toxic Effects of Various Modifications of a Nanoparticle Following Inhalation This Publication is the Final Report of the Project "Toxic Effects of Various Modifications of a Nanoparticle Following Inhalation" – Project F 2246 – On Behalf of the Federal Institute for Occupational Safety and Health. Dortmund/Berlin/Dresden. pp. 1–405.

Creutzenberg, O., Bellmann, B., Korolewitz, R., et al., 2012a. Change in agglomeration status and toxicokinetic fate of various nanoparticles *in vivo* following lung exposure in rats. Inhal. Toxicol. 24 (12), 821–830.

Creutzenberg, O., Kock, H., Schaudien, D., 2016. Translocation and biokinetic behavior of nanoscaled europium oxide particles within 5 days following an acute inhalation in rats. J. Appl. Toxicol. 36 (3), 474–478.

Creutzenberg, O.H., Ziemann, C., Hansen, T., et al., 2012b. Subacute and subchronic inhalation toxicity and dermal absorption of the nanoscaled zinc oxide Z-COTE HP1 in the rat. Toxicologist 126 (1), 142–143.

Dan, M., Tseng, M.T., Wu, P., Unrine, J.M., Grulke, E.A., Yokel, R.A., 2012a. Brain microvascular endothelial cell association and distribution of a 5 nm ceria engineered nanomaterial. Int. J. Nanomedicine 7, 4023–4036.

Dan, M., Wu, P., Grulke, E.A., Graham, U.M., Unrine, J.M., Yokel, R.A., 2012b. Ceria-engineered nanomaterial distribution in, and clearance from, blood: size matters. Nanomedicine 7 (1), 95–110.

Dankovic, D., Kuempel, E., Wheeler, M., 2007. An approach to risk assessment for TiO_2. Inhal. Toxicol. 19, 205–212.

Devine, D.V., Bradley, A.J., 1998. The complement system in liposome clearance: can complement deposition be inhibited? Adv. Drug Deliv. Rev. 32 (1–2), 19–29.

Dobrovolskaia, M.A., Patri, A.K., Zheng, J., et al., 2009. Interaction of colloidal gold nanoparticles with human blood: effects on particle size and analysis of plasma protein binding profiles. Nanomedicine 5 (2), 106–117.

Donaldson, K., Borm, P.J.A., Oberdörster, G., Pinkerton, K.E., Stone, V., Tran, C.L., 2008. Concordance between *in vitro* and *in vivo* dosimetry in the proinflammatory effects of low-toxicity, low-solubility particles: the key role of the proximal alveolar region. Inhal. Toxicol. 20 (1), 53–62.

Donaldson, K., Murphy, F.A., Duffin, R., Poland, C.A., 2010. Asbestos, carbon nanotubes and the pleural mesothelium: a review of the hypothesis regarding the role of long fibre retention in the parietal pleura, inflammation and mesothelioma. Part Fibre Toxicol 7, 5.

Donaldson, K., Poland, C.A., 2013. Nanotoxicity: challenging the myth of nano-specific toxicity. Curr. Opin. Biotechnol. 24 (4), 724–734.

Donaldson, K., Schinwald, A., Murphy, F., et al., 2013. The biologically effective dose in inhalation nanotoxicology. Acc. Chem. Res. 46 (3), 723–732.

Donaldson, K., Seaton, A., 2012. A short history of the toxicology of inhaled particles. Part Fibre Toxicol 9, 13.

Elder, A., Gelein, R., Finkelstein, J.N., Driscoll, K.E., Harkema, J., Oberdörster, G., 2005. Effects of subchronically inhaled carbon black in three species. I. Retention kinetics, lung inflammation, and histopathology. Toxicol. Sci. 88 (2), 614–629.

Ernsting, M.J., Murakami, M., Roy, A., Li, S.D., 2013. Factors controlling the pharmacokinetics, biodistribution and intratumoral penetration of nanoparticles. J. Control. Release 172 (3), 782–794.

Estrela-Lopis, I., Romero, G., Rojas, E., Moya, S.E., Donath, E., 2011. Nanoparticle uptake and their co-localization with cell compartments - a confocal Raman microscopy study at single cell level. J Phys CS 304 (1).

Fabian, E., Landsiedel, R., Ma-Hock, L., Wiench, K., Wohlleben, W., van Ravenzwaay, B., 2008. Tissue distribution and toxicity of intravenously administered titanium dioxide nanoparticles in rats. Arch. Toxicol. 82 (3), 151–157.

Fletcher, J.S., Lockyer, N.P., Vickerman, J.C., 2011. Developments in molecular SIMS depth profiling and 3D imaging of biological systems using polyatomic primary ions. Mass Spectrom. Rev. 30 (1), 142–174.

Gebel, T., Foth, H., Damm, G., et al., 2014. Manufactured nanomaterials: categorization and approaches to hazard assessment. Arch. Toxicol. 88 (12), 2191–2211.

Gebel, T., Landsiedel, R., 2013. Contents of security research: long-term effects of bio-resistant nano dust. Gefahrstoffe - Reinhalt. Luft 73 (10), 414.

Geiser, M., Kreyling, W.G., 2010. Deposition and biokinetics of inhaled nanoparticles. Part. Fibre Toxicol. 7 (2), 1–17.

Geraets, L., Oomen, A.G., Schroeter, J.D., Coleman, V.A., Cassee, F.R., 2012. Tissue distribution of inhaled micro- and nano-sized cerium oxide particles in rats: results from a 28-day exposure study. Toxicol. Sci. 127 (2), 463–473.

Giard, D.J., Aaronson, S.A., Todaro, G.J., et al., 1973. In vitro cultivation of human tumors: establishment of cell lines derived from a series of solid tumors. J. Natl. Cancer Inst. 51 (5), 1417–1423.

Graham, U.M., Tseng, M.T., Jasinski, J.B., et al., 2014. *In vivo* processing of ceria nanoparticles inside liver: impact on free-radical scavenging activity and oxidative stress. Chempluschem 79 (8), 1083–1088.

Gregoratto, D., Bailey, M.R., Marsh, J.W., 2010. Modelling particle retention in the alveolar-interstitial region of the human lungs. J. Radiol. Prot. 30 (3), 491–512.

Gulson, B., McCall, M.J., Bowman, D.M., Pinheiro, T., 2015. A review of critical factors for assessing the dermal absorption of metal oxide nanoparticles from sunscreens applied to humans, and a research strategy to address current deficiencies. Arch. Toxicol. 89 (11), 1909–1930.

Haase, A., Arlinghaus, H.F., Tentschert, J., et al., 2011. Application of laser postionization secondary neutral mass spectrometry/time-of-flight secondary ion mass spectrometry in nanotoxicology: visualization of nanosilver in human macrophages and cellular responses. ACS Nano 5 (4), 3059–3068.

Hackbarth, A., 2015. Biological effects of engineered multiwalled carbon nanotubes in the animal model and cell cultures. Doctoral Thesis, University of Veterinary Medicine, Hannover, Germany.

Hagens, W.I., Oomen, A.G., de Jong, W.H., Cassee, F.R., Sips, A.J., 2007. What do we (need to) know about the kinetic properties of nanoparticles in the body? Regul. Toxicol. Pharmacol. 49 (3), 217–229.

Hardas, S.S., Butterfield, D.A., Sultana, R., et al., 2010. Brain distribution and toxicological evaluation of a systemically delivered engineered nanoscale ceria. Toxicol. Sci. 116 (2), 562–576.

Health Effects Institute DEP, 2015. Diesel Emissions and Lung Cancer: An Evaluation of Recent Epidemiological Evidence for Quantitative Risk Assessment, Special Report 19. USA, Boston.

Heckman, K.L., DeCoteau, W., Estevez, A., et al., 2013. Custom cerium oxide nanoparticles protect against a free radical mediated autoimmune degenerative disease in the brain. ACS Nano 7 (12), 10582–10596.

Hirsch, V., Kinnear, C., Rodriguez-Lorenzo, L., et al., 2014. *In vitro* dosimetry of agglomerates. Nano 6 (13), 7325–7331.

Hirst, S.M., Karakoti, A., Singh, S., et al., 2013. Bio-distribution and *in vivo* antioxidant effects of cerium oxide nanoparticles in mice. Environ. Toxicol. 28 (2), 107–118.

Holzweber, M., Shard, A.G., Jungnickel, H., Luch, A., Unger, W.E.S., 2014. Dual beam organic depth profiling using large argon cluster ion beams. Surf. Interface Anal. 46 (10−11), 936–939.

IARC, 1997. Silica, Some Silicates, Coal Dust and Para-Aramid Fibrils IARC Monographs on the Evaluation of Carcinogenic Risks to Humans. vol 68. World Health Organization, International Agency for Research on Cancer, Lyon, France, p. 521.

IARC, 2010. Carbon Black, Titanium Dioxide, and Talc IARC Monographs on the Evaluation of Carcinogenic Risks to Humans. vol 93. World Health Organization, International Agency for Research on Cancer, Lyon.

IARC, 2014. Diesel and Gasoline Engine Exhausts and Some Nitroarenes IARC Monographs on the Evaluation of Carcinogenic Risks to Humans. vol 105. World Health Organization, International Agency for Research on Cancer, Lyon, France, p. 714.

Kambe, T., Hashimoto, A., Fujimoto, S., 2014. Current understanding of ZIP and ZnT zinc transporters in human health and diseases. Cell. Mol. Life Sci. 71 (17), 3281–3295.

Kasai, T., Umeda, Y., Ohnishi, M., et al., 2016. Lung carcinogenicity of inhaled multi-walled carbon nanotube in rats. Part Fibre Toxicol 13 (53), 1–6.

Kato, T., Yashiro, T., Murata, Y., et al., 2003. Evidence that exogenous substances can be phagocytized by alveolar epithelial cells and transported into blood capillaries. Cell Tissue Res. 311 (1), 47–51.

Keller, J., Groters, S., Ma-Hock, L., et al., 2013. Toxicology of nanomaterials: long-term inhalation study with nanomaterials: pulmonary effects of nanoscale ceriumoxide and bariumsulfate in a rat 28 day range finding study. N-S Arch Pharmacol 386, S40.

Keller, J., Wohlleben, W., Ma-Hock, L., et al., 2014. Time course of lung retention and toxicity of inhaled particles: short-term exposure to nano-ceria. Arch. Toxicol. 88 (11), 2033–2059.
Kermanizadeh, A., Balharry, D., Wallin, H., Loft, S., Moller, P., 2015. Nanomaterial translocation-the biokinetics, tissue accumulation, toxicity and fate of materials in secondary organs-a review. Crit. Rev. Toxicol. 45 (10), 837–872.
Kettiger, H., Schipanski, A., Wick, P., Huwyler, J., 2013. Engineered nanomaterial uptake and tissue distribution: from cell to organism. Int. J. Nanomedicine 8, 3255–3269.
Konduru, N., Keller, J., Ma-Hock, L., et al., 2014. Biokinetics and effects of barium sulfate nanoparticles. Part Fibre Toxicol 11 (55), 1–15.
Kreyling, W.G., Semmler, M., Erbe, F., et al., 2002. Translocation of ultrafine insoluble iridium particles from lung epithelium to extrapulmonary organs is size dependent but very low. J. Toxic. Environ. Health A 65 (20), 1513–1530.
Kreyling, W.G., Semmler-Behnke, M., Seitz, J., et al., 2009. Size dependence of the translocation of inhaled iridium and carbon nanoparticle aggregates from the lung of rats to the blood and secondary target organs. Inhal. Toxicol. 21 (Suppl. 1), 55–60.
Kreyling, W.G., Semmler-Behnke, M., Takenaka, S., Moller, W., 2013. Differences in the biokinetics of inhaled nano- versus micrometer-sized particles. Acc. Chem. Res. 46 (3), 714–722.
Kuempel, E.D., Attfield, M.D., Stayner, L.T., Castranova, V., 2014. Human and animal evidence supports lower occupational exposure limits for poorly-soluble respirable particles: Letter to the Editor re: 'Low-toxicity dusts: Current exposure guidelines are not sufficiently protective' by Cherrie, Brosseau, Hay and Donaldson. Ann. Occup. Hyg. 58 (9), 1205–1208.
Kuempel, E.D., O'Flaherty, E.J., Stayner, L.T., Smith, R.J., Green, F.H.Y., Vallyathan, V., 2001a. A biomathematical model of particle clearance and retention in the lungs of coal miners - I. Model development. Regul. Toxicol. Pharmacol. 34 (1), 69–87.
Kuempel, E.D., Tran, C.L., Smith, R.J., Bailer, A.J., 2001b. A biomathematical model of particle clearance and retention in the lungs of coal miners - II. Evaluation of variability and uncertainty. Regul. Toxicol. Pharmacol. 34 (1), 88–101.
Kumar, A., Bicer, E.M., Morgan, A.B., et al., 2016. Enrichment of immunoregulatory proteins in the biomolecular corona of nanoparticles within human respiratory tract lining fluid. Nanomedicine 12 (4), 1033–1043.
Landsiedel, R., Fabian, E., Ma-Hock, L., et al., 2012. Toxico-/biokinetics of nanomaterials. Arch. Toxicol. 86 (7), 1021–1060.
Lankveld, D.P.K., Oomen, A.G., Krystek, P., et al., 2010. The kinetics of the tissue distribution of silver nanoparticles of different sizes. Biomaterials 31 (32), 8350–8361.
Levy, L., Chaudhuri, I.S., Krueger, N., McCunney, R.J., 2012. Does carbon black disaggregate in lung fluid? A critical assessment. Chem. Res. Toxicol. 25 (10), 2001–2006.
Li, D., Johanson, G., Emond, C., Carlander, U., Philbert, M., Jolliet, O., 2014. Physiologically based pharmacokinetic modeling of polyethylene glycol-coated polyacrylamide nanoparticles in rats. Nanotoxicology 8 (Suppl. 1), 128–137.
Llop, J., Estrela-Lopis, I., Ziolo, R.F., et al., 2014. Uptake, biological fate, and toxicity of metal oxide nanoparticles. Part. Part. Syst. Charact. 31 (1), 24–35.
Lundqvist, M., Stigler, J., Elia, G., Lynch, I., Cedervall, T., Dawson, K.A., 2008. Nanoparticle size and surface properties determine the protein corona with possible implications for biological impacts. Proc. Natl. Acad. Sci. U. S. A. 105 (38), 14265–14270.
MacCalman, L., Tran, C.L., 2009. Development and Extension of a Bio-Mathematical Model in Rats to Describe Particle Size-Specific Clearance and Translocation of Inhaled Particles and Early Biological Responses. Institute of Occupational Medicine Research Report TM/09/03.
MacCalman, L., Tran, C.L., Kuempel, E., 2009. Development of a bio-mathematical model in rats to describe clearance, retention and translocation of inhaled nano particles throughout the body. J. Phys. Conf. Ser. 151. http://iopscience.iop.org/article/10.1088/1742-6596/151/1/012028/pdf (Accessed 24.02.2017).
Ma-Hock, L., Keller, J., Groeters, S., Strauss, V., van Ravenzwaay, B., Landsiedel, R., 2014. A life-time inhalation carcinogenicity study with two nano materials. Mutagenesis 29 (6), 530.
MAK Commission, 2014. The MAK-collection part I, MAK value documentations 2014. In: Forschungsgemeinschaft, Deutsche (Ed.), The MAK Collection for Occupational Health and Safety. Wiley-VCH Verlag GmbH & Co, KGaA, p. 320.
Matthaus, C., Kale, A., Chernenko, T., Torchilin, V., Diem, M., 2008. New ways of imaging uptake and intracellular fate of liposomal drug carrier systems inside individual cells, based on Raman microscopy. Mol. Pharm. 5 (2), 287–293.
Mauderly, J.L., 1997. Relevance of particle-induced rat lung tumors for assessing lung carcinogenic hazard and human lung cancer risk. Environ. Health Perspect. 105 (Suppl. 5), 1337–1346.
Mercer, R.R., Scabilloni, J.F., Hubbs, A.F., et al., 2013. Distribution and fibrotic response following inhalation exposure to multi-walled carbon nanotubes. Part Fibre Toxicol 10 (33), 1–14.
Methner, M., Hodson, L., Dames, A., Geraci, C., 2010. Nanoparticle emission assessment technique (NEAT) for the identification and measurement of potential inhalation exposure to engineered nanomaterials-part B: results from 12 field studies. J. Occup. Environ. Hyg. 7 (3), 163–176.
Meuller, B.O., Messing, M.E., Engberg, D.L.J., et al., 2012. Review of spark discharge generators for production of nanoparticle aerosols. Aerosol Sci. Technol. 46 (11), 1256–1270.
Mitrano, D.M., Motellier, S., Clavaguera, S., Nowack, B., 2015. Review of nanomaterial aging and transformations through the life cycle of nano-enhanced products. Environ. Int. 77, 132–147.
Moghimi, S.M., Hunter, A.C., Murray, J.C., 2001. Long-circulating and target-specific nanoparticles: theory to practice. Pharmacol. Rev. 53 (2), 283–318.
Molina, R.M., Konduru, N.V., Jimenez, R.J., et al., 2014. Bioavailability, distribution and clearance of tracheally instilled, gavaged or injected cerium dioxide nanoparticles and ionic cerium. Environ. Sci.: Nano 1 (6), 561–573.
Monopoli, M.P., Aberg, C., Salvati, A., Dawson, K.A., 2012. Biomolecular coronas provide the biological identity of nanosized materials. Nat. Nanotechnol. 7 (12), 779–786.
Monopoli, M.P., Walczyk, D., Campbell, A., et al., 2011. Physical-chemical aspects of protein corona: relevance to *in vitro* and *in vivo* biological impacts of nanoparticles. J. Am. Chem. Soc. 133 (8), 2525–2534.
Moreno-Horn, M., Gebel, T., 2014. Granular biodurable nanomaterials: no convincing evidence for systemic toxicity. Crit. Rev. Toxicol. 44 (10), 849–875.
Morfeld, P., Treumann, S., Ma-Hock, L., Bruch, J., Landsiedel, R., 2012. Deposition behavior of inhaled nanostructured TiO_2 in rats: fractions of particle diameter below 100 nm (nanoscale) and the slicing bias of transmission electron microscopy. Inhal. Toxicol. 24 (14), 939–951.
Morrow, P.E., 1988. Possible mechanisms to explain dust overloading of the lungs. Fundam. Appl. Toxicol. 10 (3), 369–384.
NANoREG, 2013. A Common European Approach to the Regulatory Testing of Manufactured Nanomaterials. http://www.nanoreg.eu (Accessed 13.01.2017).
NANoREG, 2015a. Long Term Inhalation Study, Deliverable 4.1. http://www.nanoreg.eu/media-and-downloads/factsheets-of-nanoreg-output/242-deliverable-4-1-long-term-inhalation-study (Accessed 13.01.2017).
NANoREG, 2015b. Lung Burden After Sub-Acute Exposure, Deliverable 4.3. http://www.nanoreg.eu/images/2015_09_10_NANoREG_Factsheet_D4.3.pdf (Accessed 13.01.2017).
NANoREG, 2015c. Organ Burden and Particle Detection Pattern on Other Organs After Subacute Exposure, Deliverable 4.4. http://www.nanoreg.eu/images/2015_09_08_NANoREG_Factsheet_D4.4.pdf (Accessed 13.01.2017).
Neale, P.A., Jamting, A.K., Escher, B.I., Herrmann, J., 2013. A review of the detection, fate and effects of engineered nanomaterials in wastewater treatment plants. Water Sci. Technol. 68 (7), 1440–1453.
Nemmar, A., Hoylaerts, M.F., Hoet, P.H., Nemery, B., 2004. Possible mechanisms of the cardiovascular effects of inhaled particles: systemic translocation and prothrombotic effects. Toxicol. Lett. 149 (1–3), 243–253.
Nikula, K.J., Avila, K.J., Griffith, W.C., Mauderly, J.L., 1997. Lung tissue responses and sites of particle retention differ between rats and cynomolgus monkeys exposed chronically to diesel exhaust and coal dust. Fundam. Appl. Toxicol. 37 (1), 37–53.
Nikula, K.J., Vallyathan, V., Green, F.H., Hahn, F.F., 2001. Influence of exposure concentration or dose on the distribution of particulate material in rat and human lungs. Environ. Health Perspect. 109 (4), 311–318.
Oberdörster, G., 1989. Dosimetric principles for extrapolating results of rat inhalation studies to humans, using an inhaled Ni compound as an example. Health Phys. 57 (Suppl. 1), 213–220.
Oberdörster, G., Cox, C., Gelein, R., 1997. Intratracheal instillation versus intratracheal-inhalation of tracer particles for measuring lung clearance function. Exp. Lung Res. 23 (1), 17–34.
Oberdörster, G., Ferin, J., Gelein, R., Soderholm, S.C., Finkelstein, J., 1992a. Role of the alveolar macrophage in lung injury: studies with ultrafine particles. Environ. Health Perspect. 97, 193–199.
Oberdörster, G., Ferin, J., Lehnert, B.E., 1994. Correlation between particle-size, in-vivo particle persistence, and lung injury. Environ. Health Perspect. 102, 173–179.
Oberdörster, G., Ferin, J., Morrow, P.E., 1992b. Volumetric loading of alveolar macrophages (AM): a possible basis for diminished AM-mediated particle clearance. Exp. Lung Res. 18 (1), 87–104.
Oberdörster, G., Oberdörster, E., Oberdörster, J., 2005. Nanotoxicology: an emerging discipline evolving from studies of ultrafine particles. Environ. Health Perspect. 113 (7), 823–839.
OECD, 2016. Testing Programme of Manufactured Nanomaterials. http://www.oecd.org/chemicalsafety/nanosafety/testing-programme-manufactured-nanomaterials.htm (Accessed 13.01.2017).
Pauluhn, J., 2009a. Comparative pulmonary response to inhaled nanostructures: considerations on test design and endpoints. Inhal. Toxicol. 21 (Suppl. 1), 40–54.
Pauluhn, J., 2009b. Pulmonary toxicity and fate of agglomerated 10 and 40 nm aluminum oxyhydroxides following 4-week inhalation exposure of rats: toxic effects are determined by agglomerated, not primary particle size. Toxicol. Sci. 109 (1), 152–167.
Pauluhn, J., 2011. Poorly soluble particulates: searching for a unifying denominator of nanoparticles and fine particles for DNEL estimation. Toxicology 279 (1–3), 176–188.
Pauluhn, J., 2014a. Derivation of occupational exposure levels (OELs) of low-toxicity isometric biopersistent particles: how can the kinetic lung overload paradigm be used for improved inhalation toxicity study design and OEL-derivation? Part Fibre Toxicol 11 (72), 1–14.
Pauluhn, J., 2014b. Repeated inhalation exposure of rats to an anionic high molecular weight polymer aerosol: application of prediction models to better understand pulmonary effects and modes of action. Exp. Toxicol. Pathol. 66 (5–6), 243–256.
Petros, R.A., DeSimone, J.M., 2010. Strategies in the design of nanoparticles for therapeutic applications. Nat. Rev. Drug Discov. 9 (8), 615–627.
Preining, O., 1998. The physical nature of very, very small particles and its impact on their behaviour. J. Aerosol Sci. 29 (5–6), 481–495.
Reinert, T., Andrea, T., Barapatre, N., et al., 2011. Biomedical research at LIPSION - present state and future developments. Nucl Instrum Meth B 269 (20), 2254–2259.
Riviere, J.E., 2009. Pharmacokinetics of nanomaterials: an overview of carbon nanotubes, fullerenes and quantum dots. Wiley Interdiscip Rev Nanomed Nanobiotechnol 1 (6), 685.
Rojas, S., Gispert, J.D., Abad, S., et al., 2012. In vivo biodistribution of amino-functionalized ceria nanoparticles in rats using positron emission tomography. Mol. Pharm. 9, 3543–3550.
Roller, M., 2003. Dose-response relationships of granular bio-durable dusts in rat lungs: does a cancer threshold exist? Eur J Oncol 8 (4), 277–293.
Roller, M., Pott, F., 2006. Lung tumor risk estimates from rat studies with not specifically toxic granular dusts. Ann. N. Y. Acad. Sci. 1076, 266–280.
Romero, G., Estrela-Lopis, I., Castro-Hartmann, P., et al., 2011a. Stepwise surface tailoring of carbon nanotubes with polyelectrolyte brushes and lipid layers to control their intracellular distribution and "in vitro" toxicity. Soft Matter 7 (15), 6883–6890.

Romero, G., Estrela-Lopis, I., Zhou, J., et al., 2010. Surface engineered poly(lactide-co-glycolide) nanoparticles for intracellular delivery: uptake and cytotoxicity–a confocal Raman microscopic study. Biomacromolecules 11 (11), 2993–2999.
Romero, G., Ochoteco, O., Sanz, D.J., Estrela-Lopis, I., Donath, E., Moya, S.E., 2013. Poly(lactide-co-glycolide) nanoparticles, layer by layer engineered for the sustainable delivery of antiTNF-alpha. Macromol. Biosci. 13 (7), 903–912.
Romero, G., Rojas, E., Estrela-Lopis, I., Donath, E., Moya, S.E., 2011b. Spontaneous confocal Raman microscopy–a tool to study the uptake of nanoparticles and carbon nanotubes into cells. Nanoscale Res. Lett. 6, 429.
Sa, L.T.M., Albernaz, M.D., Patricio, B.F.D., et al., 2012. Biodistribution of nanoparticles: initial considerations. J Pharmaceut Biomed 70, 602–604.
Sargent, L.M., Porter, D.W., Staska, L.M., et al., 2014. Promotion of lung adenocarcinoma following inhalation exposure to multi-walled carbon nanotubes. Part Fibre Toxicol 11 (3), 1–17.
Schenker, M.B., 1980. Diesel exhaust - occupational carcinogen. J. Occup. Environ. Med. 22 (1), 41–46.
Schmid, O., Stoeger, T., 2016. Surface area is the biologically most effective dose metric for acute nanoparticle toxicity in the lung. J. Aerosol Sci. 99, 133–143.
Seipenbusch, M., Binder, A., Kasper, G., 2008. Temporal evolution of nanoparticle aerosols in workplace exposure. Ann. Occup. Hyg. 52 (8), 707–716.
Semmler, M., Seitz, J., Erbe, F., et al., 2004. Long-term clearance kinetics of inhaled ultrafine insoluble iridium particles from the rat lung, including transient translocation into secondary organs. Inhal. Toxicol. 16 (6–7), 453–459.
Semmler-Behnke, M., Takenaka, S., Fertsch, S., et al., 2007. Efficient elimination of inhaled nanoparticles from the alveolar region: evidence for interstitial uptake and subsequent reentrainment onto airway epithelium. Environ. Health Perspect. 115 (5), 728–733.
Senior, J., Gregoriadis, G., 1982. Is half-life of circulating liposomes determined by changes in their permeability. FEBS Lett. 145 (1), 109–114.
Silge, A., Brautigam, K., Bocklitz, T., et al., 2015. ZrO_2 nanoparticles labeled via a native protein corona: detection by fluorescence microscopy and Raman microspectroscopy in rat lungs. Analyst 140 (15), 5120–5128.
Srinivas, A., Rao, P.J., Selvam, G., Murthy, P.B., Reddy, P.N., 2011. Acute inhalation toxicity of cerium oxide nanoparticles in rats. Toxicol. Lett. 205 (2), 105–115.
Subramanian, M.S., Oomen, I.K., 1981. Complex Formation of Transferrin With Tetravalent Plutonium and Cerium. Vol BARC—1139. Bhabha Atomic Research Centre, Bombay, India, p. 12.
Sweeney, L.M., MacCalman, L., Haber, L.T., Kuempel, E.D., Tran, C.L., 2015. Bayesian evaluation of a physiologically-based pharmacokinetic (PBPK) model of long-term kinetics of metal nanoparticles in rats. Regul. Toxicol. Pharmacol. 73 (1), 151–163.
Szakal, C., Roberts, S.M., Westerhoff, P., et al., 2014. Measurement of nanomaterials in foods: integrative consideration of challenges and future prospects. ACS Nano 8 (4), 3128–3135.
Takenaka, S., Karg, E., Roth, C., et al., 2001. Pulmonary and systemic distribution of inhaled ultrafine silver particles in rats. Environ. Health Perspect. 109, 547–551.
Tenzer, S., Docter, D., Rosfa, S., et al., 2011. Nanoparticle size is a critical physicochemical determinant of the human blood plasma corona: a comprehensive quantitative proteomic analysis. ACS Nano 5 (9), 7155–7167.
Thyssen, J.P., Menne, T., Johansen, J.D., 2009. Nickel release from inexpensive jewelry and hair clasps purchased in an EU country - are consumers sufficiently protected from nickel exposure? Sci. Total Environ. 407 (20), 5315–5318.
Torchilin, V.P., 1998. In vitro and in vivo availability of liposomes. In: Kabanov, A.V., Felgner, P.L., Seymour, L.W. (Eds.), Self-Assembling Complexes for Gene Delivery: From Laboratory to Clinical Trial. John Wiley, Chichester, New York, Weinheim, Brisbane, Singapore, Toronto, pp. 277–293.
Tran, C.L., Kuempel, E.D., Castranova, V., 2002. A rat lung model of exposure, dose and response to inhaled silica. Ann. Occup. Hyg. 46 (Supplement 1), 14–17.
Tseng, M.T., Lu, X., Duan, X., et al., 2012. Alteration of hepatic structure and oxidative stress induced by intravenous nanoceria. Toxicol. Appl. Pharmacol. 260 (2), 173–182.
U.S. EPA, 2002. Health assessment document for diesel engine exhaust. In: NCfE (Ed.), Assessment. EPA/600/8-90/057F, p. 669.
Vance, M.E., Kuiken, T., Vejerano, E.P., et al., 2015. Nanotechnology in the real world: redeveloping the nanomaterial consumer products inventory. Beilstein J. Nanotechnol. 6, 1769–1780.
Vinogradov, S.V., Bronich, T.K., Kabanov, A.V., 2002. Nanosized cationic hydrogels for drug delivery: preparation, properties and interactions with cells. Adv. Drug Deliv. Rev. 54 (1), 135–147.
Watson, C.Y., Damiani, F., Ram-Mohan, S., et al., 2016. Screening for chemical toxicity using cryopreserved precision cut lung slices. Toxicol. Sci. 150 (1), 225–233.
Weibel, E.R., 1979. Morphometry of the human lung: the state of the art after two decades. Bull. Eur. Physiopathol. Respir. 15 (5), 999–1013.
Whitwell, H., Mackay, R.M., Elgy, C., et al., 2016. Nanoparticles in the lung and their protein corona: the few proteins that count. Nanotoxicology 10 (9), 1385–1394.
Yokel, R.A., Au, T.C., MacPhail, R., et al., 2012. Distribution, elimination, and biopersistence to 90 days of a systemically introduced 30 nm ceria-engineered nanomaterial in rats. Toxicol. Sci. 127 (1), 256–268.
Yokel, R.A., Florence, R.L., Unrine, J.M., et al., 2009. Biodistribution and oxidative stress effects of a systemically-introduced commercial ceria engineered nanomaterial. Nanotoxicology 3 (3), 234–248.
Yokel, R.A., Hussain, S., Garantziotis, S., Demokritou, P., Castranova, V., Cassee, F.R., 2014a. The Yin: an adverse health perspective of nanoceria: uptake, distribution, accumulation, and mechanisms of its toxicity. Environ. Sci. Nano 1 (5), 406–428.
Yokel, R.A., Tseng, M.T., Dan, M., et al., 2013. Biodistribution and biopersistence of ceria engineered nanomaterials: size dependence. Nanomedicine 9 (3), 398–407.
Yokel, R.A., Unrine, J.M., Wu, P., Wang, B., Grulke, E.A., 2014b. Nanoceria biodistribution and retention in the rat after its intravenous administration are not greatly influenced by dosing schedule, dose, or particle shape. Environ. Sci.: Nano 1 (6), 549–560.
Yu, M.X., Zheng, J., 2015. Clearance pathways and tumor targeting of imaging nanoparticles. ACS Nano 9 (7), 6655–6674.
Zende-Del, A., Ahmadvand, H., Abdollah-Pour, F., et al., 2013. Cerium lanthanide effect on growth of AGS cell line with the presence of transferrin in vitro. Zahedan Journal of Research in Medical Sciences 15 (10), 41–44.
Zhang, H., Burnum, K.E., Luna, M.L., et al., 2011. Quantitative proteomics analysis of adsorbed plasma proteins classifies nanoparticles with different surface properties and size. Proteomics 11 (23), 4569–4577.
Zhou, X., Dorn, M., Vogt, J., et al., 2014. A quantitative study of the intracellular concentration of graphene/noble metal nanoparticle composites and their cytotoxicity. Nano 6 (15), 8535–8542.